Empirical transverse charge densities in the nucleon-to-$P_{11}(1440)$ transition

Lothar Tiator and Marc Vanderhaeghen

Institut für Kernphysik, Johannes Gutenberg-Universität, D-55099 Mainz, Germany

(Dated: November 14, 2008)

Abstract

Using recent experimental data, we analyze the electromagnetic transition from the nucleon to the $P_{11}(1440)$ resonance. From the resulting empirical transition form factors, we map out the quark transverse charge densities which induce the $N \to P_{11}(1440)$ transition. It is found that the transition from the proton to its first radially excited state is dominated by up quarks in a central region of around 0.5 fm and by down quarks in an outer band which extends up to about 1 fm.

A major focuss of current research in hadronic physics centers around the question of how the structure of the nucleon and its excitations can be quantitatively understood from the interaction among its constituent quarks and gluons. To this end, a substantial experimental effort is underway at electron facilities such as JLab, ELSA, and MAMI to map out the nucleon excitation spectrum and to measure the electromagnetic transition form factors from a nucleon to an excited baryon.

The form factors (FFs) describing the electromagnetic (e.m.) transition of the nucleon to the first baryon excitation, the $\Delta(1232)$ resonance, have been measured precisely and over a large range of photon virtualities by means of the $ep \to ep\pi^0$ and $ep \to en\pi^+$ reaction. The resulting data allow to study and quantify the deformation of the $N \to \Delta$ transition charge distribution, see e.g. Ref. [1] for a recent review and references therein.

High precision data have also become available in recent years for the $\gamma^* N \to N^*$ transition, for the $P_{11}(1440)$ [3, 4, 5, 6], $D_{13}(1520)$ [3, 4, 5], $S_{11}(1535)$ [3, 4, 5, 7] and $F_{15}(1680)$ [3, 4] nucleon resonances, from π^0 [8, 9], π^+ [10, 11, 12], and η [7, 13, 14, 15] electroproduction data on the nucleon.

On the theoretical side, the nucleon-to-resonance transition FFs are also becoming amenable to lattice QCD calculations. For the $N \to \Delta$ transition, first full QCD results using different fermion actions were presented in Ref. [16]. It was found that the unquenched results for the small $N \to \Delta$ Coulomb quadrupole FF show deviations from the unquenched one at low Q^2, underlining the important role of the pion cloud to this observable. For the electromagnetic transition of the nucleon to its first excited state with quantum numbers $J^P = \frac{1}{2}^+$, the $P_{11}(1440)$ resonance, often referred to as the *Roper* resonance, first full QCD lattice studies were performed in Ref. [17]. The Roper resonance, being the first radial excitation of the nucleon, presents a particular challenge for lattice calculations to reproduce the correct level ordering with its negative-parity partner, the $S_{11}(1535)$ resonance.

The precise e.m. FF data, extracted from experiment, allow to map out the quark charge densities in a baryon. It was shown possible to define a proper density interpretation of the form factor data by viewing the baryon in a light-front frame. This yields information on the spatial distribution of the quark charge in the plane transverse to the line-of-sight. In this way, the quark transverse charge densities were mapped out in the nucleon [18, 19], and in the deuteron [20] based on empirical FF data. Furthermore, recent lattice QCD results were used to map out the quark transverse densities in the $\Delta(1232)$ [21] resonance. To understand

the e.m. structure of a nucleon resonance, it is of interest to use the precise transition FF data to reveal the spatial distribution of the quark charges that induce such a transition. In this way, the $N \to \Delta(1232)$ transition charge densities have been mapped out in Ref. [19] using the empirical information of the $N \to \Delta(1232)$ transition FFs [4]. In the following, we will generalize the above considerations to the e.m. transition between the nucleon and the first excited state with nucleon quantum numbers, the $P_{11}(1440)$ resonance. We will use the empirical information to map out the quark transition charge densities inducing the $N \to P_{11}(1440)$ e.m. excitation.

After outlining the definitions to characterize the vertex for the $N \to P_{11}(1440)$ e.m. transition, we will use the recent JLab/CLAS data to extract the two independent $N \to P_{11}(1440)$ transition FFs. Subsequently, we define the transition densities and use the empirical FF information to map out the spatial distribution of quark charges that induce the $N \to P_{11}(1440)$ transition. We finally give a brief summary and outline extensions of this work.

Consider the e.m. transition from the nucleon to its first excited state, the $P_{11}(1440)$ resonance, which we will denote in the following by N^*. A Lorentz-covariant decomposition of the matrix element of the electromagnetic current operator J^μ for this transition, satisfying manifest electromagnetic gauge-invariance, can be written as :

$$\langle N^*(p', \lambda') \,|\, J^\mu(0) \,|\, N(p, \lambda) \rangle = \bar{u}(p', \lambda') \left\{ F_1^{NN^*}(Q^2) \left(\gamma^\mu - \gamma \cdot q \frac{q^\mu}{q^2} \right) \right.$$
$$\left. + F_2^{NN^*}(Q^2) \frac{i\sigma^{\mu\nu} q_\nu}{(M^* + M_N)} \right\} u(p, \lambda), \qquad (1)$$

where M_N is the nucleon mass, $M^* = 1.440$ GeV is the mass of the first excited resonance with nucleon quantum numbers, λ (λ') are the initial (final) baryon helicities, and u is the spin 1/2 spinor, normalized as $\bar{u}u = 2M$. Furthermore, $F_{1,2}^{NN^*}$ are the electromagnetic (e.m.) FFs for the $N \to N^*$ transition.

Equivalently, one can also parametrize the $\gamma^* NN^*$ transition through two helicity amplitudes $A_{1/2}$ and $S_{1/2}$, which are defined in the N^* rest frame. These N^* rest frame helicity amplitudes are defined through the following matrix elements of the electromagnetic current operator:

$$A_{1/2} \equiv -\frac{e}{\sqrt{2K}} \frac{1}{(4M_N M^*)^{1/2}} \langle\, N^*(\vec{0}, +1/2) \,|\, \mathbf{J} \cdot \epsilon_{\lambda=+1} \,|\, N(-\vec{q}, -1/2) \,\rangle,$$
$$S_{1/2} \equiv \frac{e}{\sqrt{2K}} \frac{1}{(4M_N M^*)^{1/2}} \langle\, N^*(\vec{0}, +1/2) \,|\, J^0 \,|\, N(-\vec{q}, +1/2) \,\rangle, \qquad (2)$$

where the spin projections are along the z-axis (chosen along the virtual photon direction) and where the transverse photon polarization vector entering $A_{1/2}$ is given by $\epsilon_{\lambda=+1} = -1/\sqrt{2}(1, i, 0)$. Furthermore in Eq. (2), e is the proton electric charge, related to the fine-structure constant as $\alpha_{em} \equiv e^2/(4\pi) \simeq 1/137$, and K is the "equivalent photon energy" defined as :

$$K \equiv \frac{M^{*2} - M_N^2}{2M^*}.\tag{3}$$

The helicity amplitudes are functions of the photon virtuality Q^2, and can be expressed in terms of the FFs $F_1^{NN^*}$ and $F_2^{NN^*}$ as :

$$A_{1/2} = e\,\frac{Q_-}{\sqrt{K}\,(4M_N M^*)^{1/2}}\left\{F_1^{NN^*} + F_2^{NN^*}\right\},\tag{4}$$

$$S_{1/2} = e\,\frac{Q_-}{\sqrt{2K}\,(4M_N M^*)^{1/2}}\left(\frac{Q_+ Q_-}{2M^*}\right)\frac{(M^* + M_N)}{Q^2}\left\{F_1^{NN^*} - \frac{Q^2}{(M^* + M_N)^2}F_2^{NN^*}\right\},\tag{5}$$

where we introduced the shorthand notation $Q_\pm \equiv \sqrt{(M^* \pm M_N)^2 + Q^2}$.

For numerical evaluation, we will use the MAID2007 parameterization [4] for the $\gamma^* N \to P_{11}(1440)$ helicity amplitudes $A_{1/2}$ and $S_{1/2}$. They have been parameterized as :

$$A_{1/2}(Q^2) = A_{1/2}^0\left(1 + a_1 Q^2 + a_2 Q^4 + a_3 Q^8\right)e^{-a_4 Q^2},\tag{6}$$

$$S_{1/2}(Q^2) = S_{1/2}^0\left(1 + s_1 Q^2 + s_2 Q^4 + s_3 Q^8\right)e^{-s_4 Q^2}.\tag{7}$$

The improved proton fit is based on $\pi^0 p$ data from [8, 22, 23] and $\pi^+ n$ data from [10, 11, 12]. The neutron fit is based only an older pre-2000 quasi-free $\pi^- p$ data from the SAID data base [24]. The resulting values of the parameters are given in Table (I, II) for both proton and neutron.

In Fig. 1, we show the helicity amplitudes for the $\gamma^* p \to P_{11}(1440)$ transition, which have been measured up to $Q^2 \simeq 5$ GeV^2. One notices that the helicity amplitude $A_{1/2}$ for transverse photons displays a sign change from a large negative value at the real photon point to a broad positive maximum around $Q^2 \simeq 2$ GeV^2. The helicity amplitude $S_{1/2}$ for longitudinal photons stays positive and has a maximum around $Q^2 \simeq 0.6$ GeV^2.

The corresponding helicity amplitudes for the neutron are shown in Fig. 2. One sees that apart from the value at the real photon point for $A_{1/2}$, these amplitudes are yet to be measured. The MAID2007 analysis shows an $A_{1/2}$ helicity amplitude for the neutron which does not display a sign change as in the proton case.
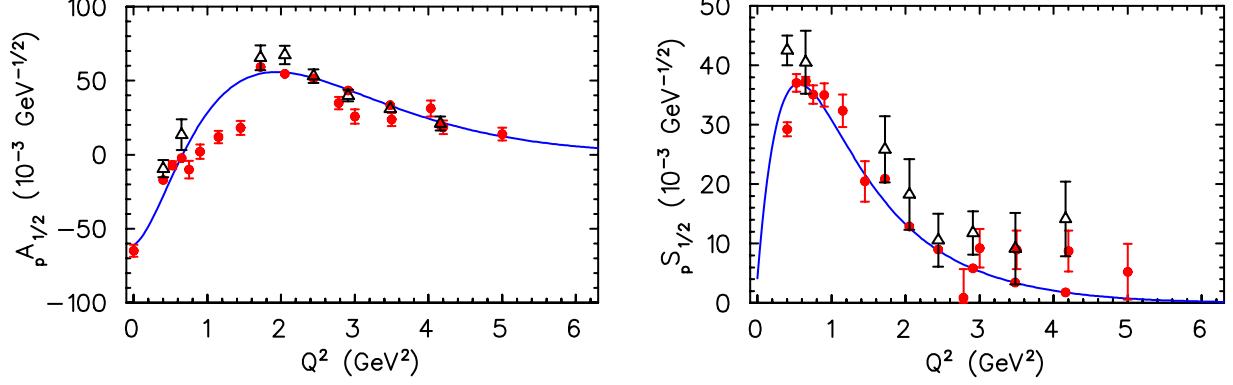
FIG. 1: Helicity amplitudes for the $\gamma^* p \to P_{11}(1440)$ transition. The solid circles are the improved MAID2007 analysis from this work. The open triangles are the analysis of Refs. [5, 6]. The point at $Q^2 = 0$ is from the PDG [25].
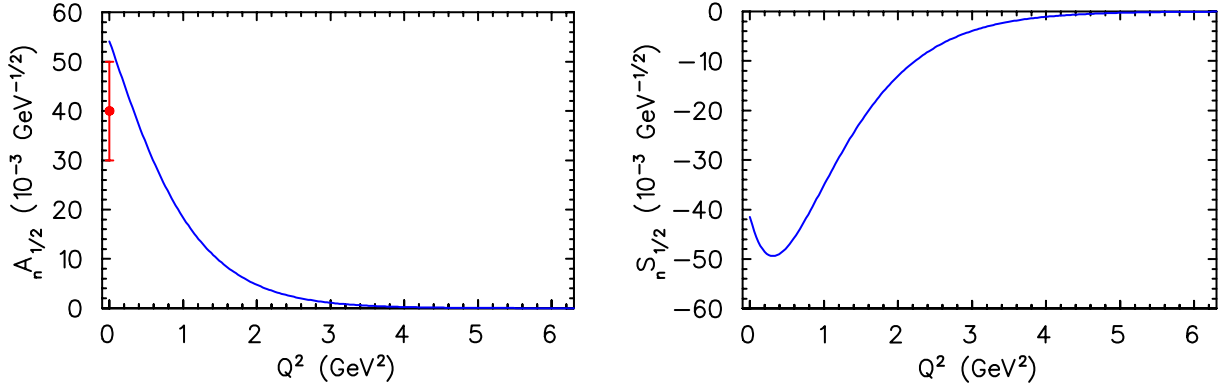

FIG. 2: Helicity amplitudes for the $\gamma^* n \to P_{11}(1440)$ transition, according to the MAID2007 [4] analysis. The point at $Q^2 = 0$ is from the PDG [25].
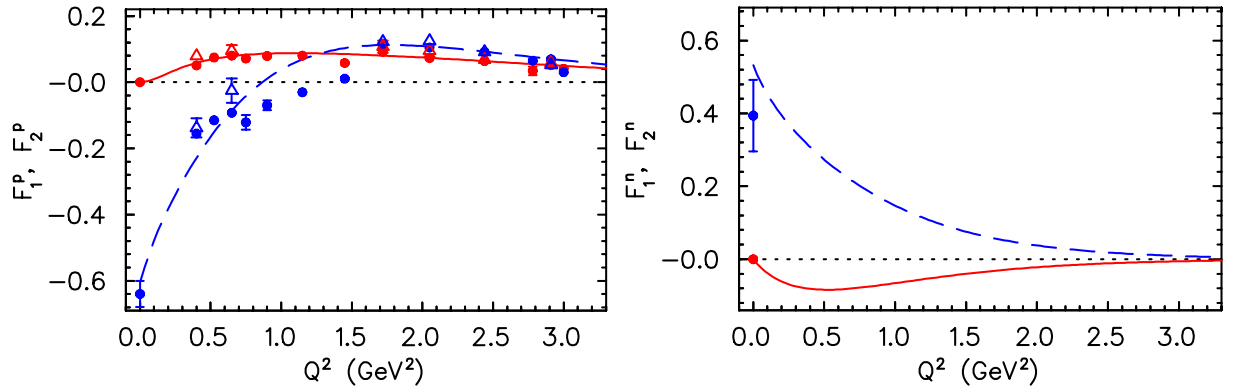

FIG. 3: Form factors for the $\gamma^* N \to P_{11}(1440)$ transition, for the proton (left panel) and the neutron (right panel), based on the MAID2007 [4] analysis for the neutron and the improved MAID2007 analysis from this work. Solid curves : $F_1^{NN^*}$; dashed curves : $F_2^{NN^*}$.

	$A^0_{1/2}$	a_1	a_2	a_3	a_4
	$(10^{-3}\ \mathrm{GeV}^{-1/2})$	(GeV^{-2})	(GeV^{-4})	(GeV^{-8})	(GeV^{-2})
p	-61.4	0.871	-3.52	-0.158	1.36
n	54.1	0.95	0	0	1.77

TABLE I: Parameters for the transverse $\gamma^* N \to P_{11}(1440)$ helicity amplitudes for the proton (first row) and for the neutron (second row), according to the MAID2007 fit [4] for the neutron, and the improved MAID2007 fit for the proton.

	$S^0_{1/2}$	s_1	s_2	s_3	s_4
	$(10^{-3}\ \mathrm{GeV}^{-1/2})$	(GeV^{-2})	(GeV^{-4})	(GeV^{-8})	(GeV^{-2})
p	4.2	40.0	0	1.5	1.75
n	-41.5	2.98	0	0	1.55

TABLE II: Parameters for the longitudinal $\gamma^* N \to P_{11}(1440)$ helicity amplitudes for the proton (first row) and for the neutron (second row), according to the MAID2007 fit for the neutron, and the improved MAID2007 fit for the proton.

In Fig. 3, we show the MAID analysis for the $\gamma^* N \to P_{11}(1440)$ transition form factors defined in Eq. (1). They are related with the helicity amplitudes as in Eq. (5). One sees that for the proton, the Dirac-like FF $F_1^{NN^*}$ vanishes with Q^2 when approaching the real photon point and stays positive at large Q^2. On the other hand, the Pauli-type FF $F_2^{NN^*}$ assumes a large negative value at the real photon point, $F_2^{pN^*}(0) = -0.64 \pm 0.04$, and changes sign around $Q^2 \simeq 1\ \mathrm{GeV}^2$.

In the following, we will consider the e.m. $N \to P_{11}(1440)$ transition when viewed from a light front moving towards the baryon. Equivalently, this corresponds with a frame where the baryons have a large momentum-component along the z-axis chosen along the direction of $P = (p + p')/2$, where p (p') are the initial (final) baryon four-momenta. We indicate the baryon light-front + component by P^+ (defining $a^\pm \equiv a^0 \pm a^3$). We can furthermore choose a symmetric frame where the virtual photon four-momentum q has $q^+ = 0$, and has a transverse component (lying in the xy-plane) indicated by the transverse vector $\vec{q}_\perp$, satisfying $q^2 = -\vec{q}_\perp^2 \equiv -Q^2$. In such a symmetric frame, the virtual photon only

6

couples to forward moving partons and the + component of the electromagnetic current J^+ has the interpretation of the quark charge density operator. It is given by : $J^+(0) = +2/3\,\bar{u}(0)\gamma^+u(0) - 1/3\,\bar{d}(0)\gamma^+d(0)$, considering only u and d quarks. Each term in the expression is a positive operator since $\bar{q}\gamma^+q \propto |\gamma^+q|^2$.

We define a transition charge density for the unpolarized $N \to N^*$ transition, by the Fourier transform :

$$\rho_0^{NN^*}(\vec{b}) \equiv \int \frac{d^2\vec{q}_\perp}{(2\pi)^2}\, e^{-i\,\vec{q}_\perp\cdot\vec{b}}\, \frac{1}{2P^+}\langle P^+, \frac{\vec{q}_\perp}{2}, \lambda\,|\,J^+(0)\,|\,P^+, -\frac{\vec{q}_\perp}{2}, \lambda\rangle, \tag{8}$$

where λ (λ') denotes the nucleon (N^*) light-front helicities, $\vec{q}_\perp = Q(\cos\phi_q\hat{e}_x + \sin\phi_q\hat{e}_y)$, and where the 2-dimensional vector $\vec{b}$ denotes the position (in the xy-plane) from the transverse c.m. of the baryons. The Fourier transform in Eq. (8) can be worked out as :

$$\rho_0^{NN^*}(\vec{b}) = \int_0^\infty \frac{dQ}{2\pi} Q\, J_0(b\,Q) F_1^{NN^*}(Q^2), \tag{9}$$

where J_n denotes the cylindrical Bessel function of order n. Note that $\rho_0^{NN^*}$ only depends on $b = |\vec{b}|$. It has the interpretation of the quark (transition) charge density in the transverse plane which induces the $N \to N^*$ excitation.

The above unpolarized transition charge density involves only one of the two independent $N \to N^*$ e.m. FFs. To extract the information encoded in $F_2^{NN^*}$, we consider the transition charge densities for a transversely polarized N and N^*. We denote this transverse polarization direction by $\vec{S}_\perp = \cos\phi_S\hat{e}_x + \sin\phi_S\hat{e}_y$. The transverse spin state can be expressed in terms of the light front helicity spinor states as : $|s_\perp = +\frac{1}{2}\rangle = \left(|\lambda = +\frac{1}{2}\rangle + e^{i\phi_S}|\lambda = -\frac{1}{2}\rangle\right)/\sqrt{2}$, with $s_\perp$ the nucleon spin projection along the direction of $\vec{S}_\perp$.

We can then define a transition charge density for a transversely polarized N and N^*, both along the direction of $\vec{S}_\perp$ as :

$$\rho_T^{NN^*}(\vec{b}) \equiv \int \frac{d^2\vec{q}_\perp}{(2\pi)^2}\, e^{-i\,\vec{q}_\perp\cdot\vec{b}}\, \frac{1}{2P^+}\langle P^+, \frac{\vec{q}_\perp}{2}, s_\perp\,|\,J^+(0)\,|\,P^+, -\frac{\vec{q}_\perp}{2}, s_\perp\rangle. \tag{10}$$

Using Eqs. (1) and (9), the Fourier transform of Eq. (10) can be worked out as :

$$\rho_T^{NN^*}(\vec{b}) = \rho_0^{NN^*}(b) + \sin(\phi_b - \phi_S) \int_0^\infty \frac{dQ}{2\pi} \frac{Q^2}{(M^* + M_N)} J_1(b\,Q) F_2^{NN^*}(Q^2), \tag{11}$$

where the second term, which describes the deviation from the circular symmetric unpolarized charge density, depends on the orientation of $\vec{b} = b(\cos\phi_b\hat{e}_x + \sin\phi_b\hat{e}_y)$. In the following we choose the transverse spin along the x-axis ($\Phi_S = 0$).
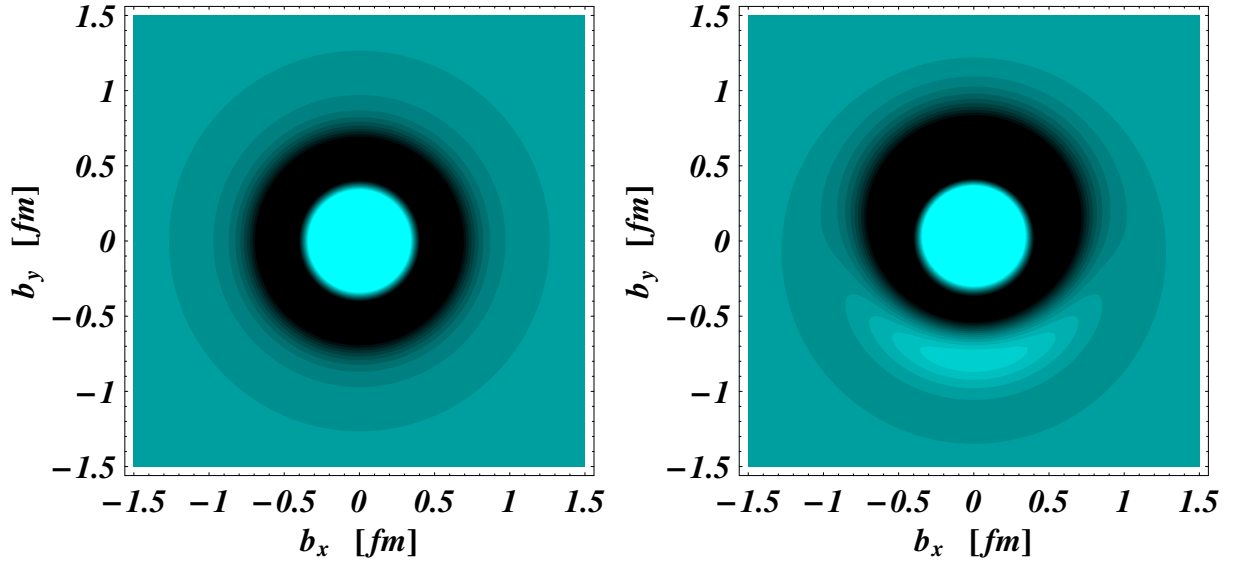
FIG. 4: Quark transverse charge density corresponding to the $p \to P_{11}(1440)$ e.m. transition. Upper left panel : when p and N^* are unpolarized ($\rho_0^{pN^*}$). Upper right panel : when p and N^* are polarized along the x-axis ($\rho_T^{pN^*}$). The light (dark) regions correspond with positive (negative) densities. Lower panel : densities $\rho_T^{pN^*}$ (solid curves) and $\rho_0^{pN^*}$ (dashed curves) along the y-axis. For the $p \to P_{11}(1440)$ e.m. transition FFs, we use the improved MAID2007 fit of this work.

We show the results for the $N \to P_{11}(1440)$ transition charge densities both for the unpolarized case and for the case of transverse polarization in Fig. 4 for the proton and in Fig 5 for the neutron. We use the empirical information on the $N \to N^*(1440)$ transition FFs as parameterized in Table (I, II) and shown in Fig. 3.
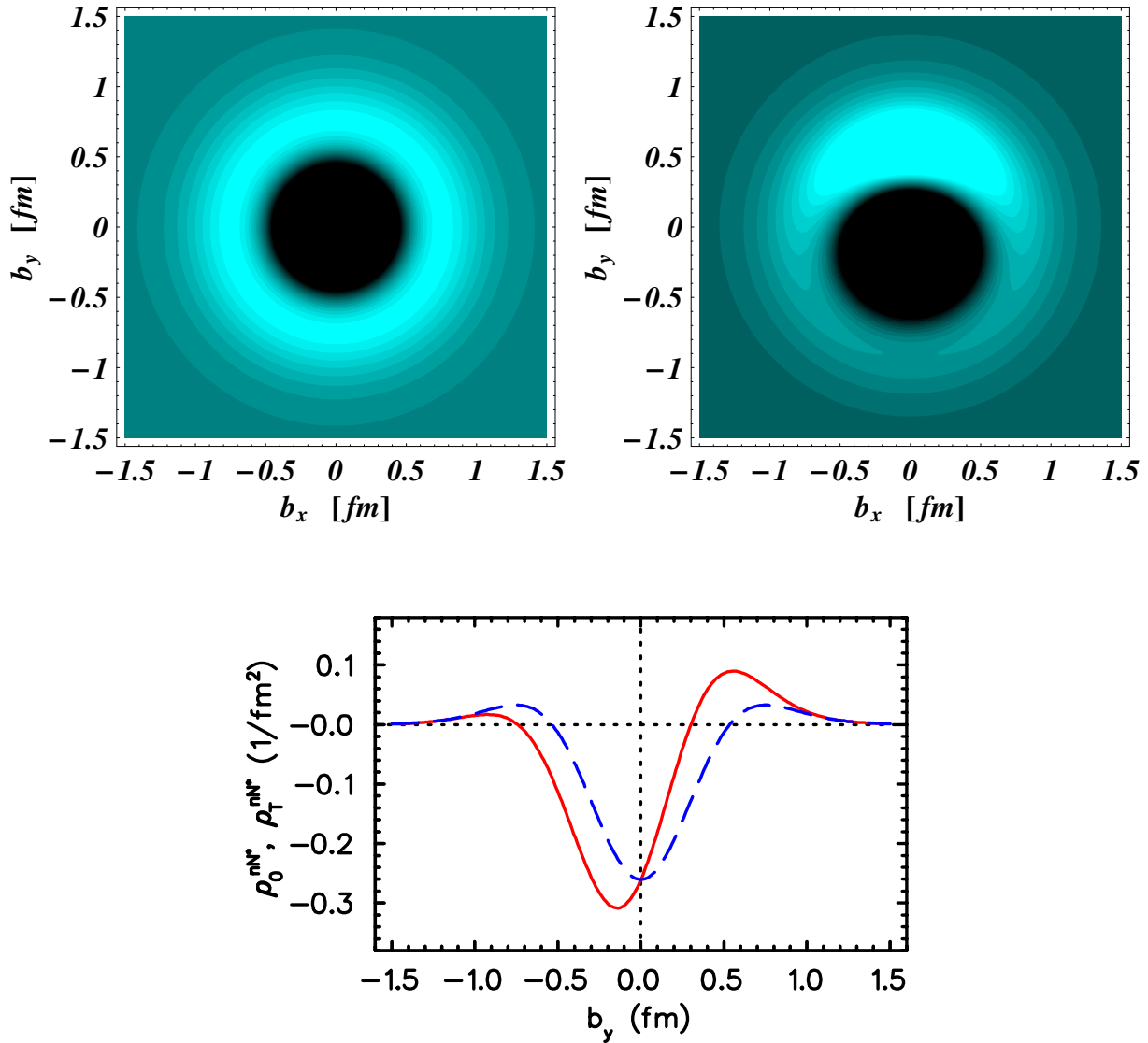
FIG. 5: Quark transverse charge density corresponding to the $n \to P_{11}(1440)$ e.m. transition. Upper left panel : when n and N^* are unpolarized ($\rho_0^{nN^*}$). Upper right panel : when n and N^* are polarized along the x-axis ($\rho_T^{nN^*}$). The light (dark) regions correspond with positive (negative) densities. Lower panel : densities $\rho_T^{nN^*}$ (solid curves) and $\rho_0^{nN^*}$ (dashed curves) along the y-axis. For the $n \to P_{11}(1440)$ e.m. transition FFs, we use the MAID2007 fit [4].

It is seen from Fig. 4 that for the transition on a proton, which is well constrained by data, there is an inner region of positive quark charge concentrated within 0.5 fm, accompanied by a relatively broad band of negative charge extending out to about 1 fm. When polarizing the baryon in the transverse plane, the large value of the magnetic transition strength at

the real photon point, yields a sizeable shift of the charge distribution, inducing an electric dipole moment. For the neutron, which is not very well constrained by data, the MAID2007 analysis yields charge distributions of opposite sign compared to the proton, with active quarks spreading out over even larger spatial distances, see Fig. 5.

It may be of interest to also extract these densities within baryon structure models, and check that within such models the quarks active in the e.m. transition from the nucleon to its first radial excited state are spatially more spread out than e.g. is the case for the e.m. $N \to \Delta$ transition.

In summary, we analyzed in the present work the e.m. $N \to P_{11}(1440)$ transition based on recent data for the proton which extend up to 5 GeV^2. We extracted both the helicity amplitudes as well as the transition form factors. The latter were used to extract the quark transverse charge densities inducing this transition. For the proton, it was found that this transition from the nucleon to its first radially excited state is dominated by up quarks in a central region of around 0.5 fm and by down quarks in an outer band which extends up to about 1 fm. We leave it as a topic for future work to extend the present analysis to also map out the quark charge densities for the $N \to S_{11}(1535)$ and $N \to D_{13}(1520)$ transitions, which have also been studied extensively in experiment.

Acknowledgments

[1] V. Pascalutsa, M. Vanderhaeghen, and S. N. Yang, Phys. Rept. **437**, 125 (2007).

[2] V. D. Burkert and T. S. H. Lee, Int. J. Mod. Phys. E **13**, 1035 (2004).

[3] L. Tiator, D. Drechsel, S. Kamalov, M. M. Giannini, E. Santopinto and A. Vassallo, Eur. Phys. J. A **19**, 55 (2004).

[4] D. Drechsel, S. S. Kamalov and L. Tiator, Eur. Phys. J. A **34**, 69 (2007).

[5] I. G. Aznauryan, V. D. Burkert, H. Egiyan, K. Joo, R. Minehart and L. C. Smith, Phys. Rev. C **71**, 015201 (2005).

[6] I. G. Aznauryan *et al.* [CLAS Collaboration], Phys. Rev. C **78**, 045209 (2008).

[7] H. Denizli *et al.* [CLAS Collaboration], Phys. Rev. C **76**, 015204 (2007).

[8] K. Joo *et al.* [CLAS Collaboration], Phys. Rev. C **72**, 058202 (2005).

[9] A. S. Biselli *et al.*, Phys. Rev. C **78**, 045204 (2008).

[10] K. Joo *et al.* [CLAS Collaboration], Phys. Rev. C **70**, 042201 (2004).

[11] H. Egiyan *et al.* [CLAS Collaboration], Phys. Rev. C **73**, 025204 (2006).

[12] K. Park *et al.* [CLAS Collaboration], Phys. Rev. C **77**, 015208 (2008).

[13] C. S. Armstrong *et al.* [Jefferson Lab E94014 Collaboration], Phys. Rev. D **60**, 052004 (1999).

[14] R. Thompson *et al.* [CLAS Collaboration], Phys. Rev. Lett. **86**, 1702 (2001).

[15] H. Merkel *et al.* [A1 Collaboration], Phys. Rev. Lett. **99**, 132301 (2007).

[16] C. Alexandrou, G. Koutsou, H. Neff, J. W. Negele, W. Schroers and A. Tsapalis, Phys. Rev. D **77**, 085012 (2008).

[17] H. W. Lin, S. D. Cohen, R. G. Edwards and D. G. Richards, arXiv:0803.3020 [hep-lat].

[18] G. A. Miller, Phys. Rev. Lett. **99**, 112001 (2007).

[19] C. E. Carlson and M. Vanderhaeghen, Phys. Rev. Lett. **100**, 032004 (2008).

[20] C. E. Carlson and M. Vanderhaeghen, arXiv:0807.4537 [hep-ph].

[21] C. Alexandrou *et al.*, arXiv:0810.3976 [hep-lat].

[22] V. V. Frolov *et al.*, Phys. Rev. Lett. **82**, 45 (1999).

[23] M. Ungaro *et al.* [CLAS Collaboration], Phys. Rev. Lett. **97**, 112003 (2006).

[24] R.A. Arndt, W.J. Briscoe, I.I. Strakovsky, R.L. Workman, http://gwdac.phys.gwu.edu/.

[25] C. Amsler *et al.* [Particle Data Group], Phys. Lett. B **667**, 1 (2008).